Journal of Applied Physics

RESEARCH ARTICLE | JUNE 20 2003

Determination of crystallite size in a magnetic nanocomposite using extended x-ray absorption fine structure

S. Calvin; M. M. Miller; R. Goswami; S.-F. Cheng; S. P. Mulvaney; L. J. Whitman; V. G. Harris

J. Appl. Phys. 94, 778–783 (2003)
https://doi.org/10.1063/1.1581344

AIP Publishing

Determination of crystallite size in a magnetic nanocomposite using extended x-ray absorption fine structure

S. Calvin,[a] M. M. Miller, R. Goswami,[b] S.-F. Cheng, S. P. Mulvaney, L. J. Whitman, and V. G. Harris
U.S. Naval Research Laboratory, Washington, DC 20375

(Received 20 February 2003; accepted 17 April 2003)

An extended x-ray absorption fine structure was collected for a soft magnetic material comprising very fine nanoscale crystallites of nickel within coarser iron matrix grains. Using a simple spherical model and the spectra of bulk standards, the nickel crystallite size was estimated. Comparison with transmission electron microscopy images confirms that this technique yields a size weighted toward smaller crystallites, whereas Scherrer analysis yields sizes weighted toward larger crystallites. The iron crystallite size was also estimated by this technique in order to ascertain the effect of a nonspherical morphology. This technique shows promise for *in situ* analyses of materials containing nanoscale crystallites and as a complement to Scherrer analyses. © *2003 American Institute of Physics.* [DOI: 10.1063/1.1581344]

I. INTRODUCTION

In recent years, considerable effort has been devoted to the synthesis and characterization of nanocrystalline soft magnetic materials.[1] It is therefore important to have a variety of tools available for probing the length scale of individual crystal domains within a material. Electron microscopy is a favored technique for this purpose, but obtaining measurements on a sufficient number of crystallites to derive a statistically meaningful average length scale is often tedious. For time-resolved *in situ* studies, in particular, electron microscopy may be prohibitively difficult. Techniques such as dynamic light scattering[2] (DLS) and Brunauer–Emmet–Teller analysis[3] (BET), on the other hand, yield the size of physical particles (i.e., powder particles), rather than individual crystalline grains embedded in a solid matrix. Scherrer analysis[4] of x-ray diffractograms is often used, but is difficult to apply when Bragg peaks of different phases within the material overlap, as in the case, for example, when separate domains of face-centered-cubic (fcc) nickel and cobalt are both present. It is also important to note that most methods of determining crystallite ''size'' find a mean diameter, with a weighting scheme that depends on the technique being used. Because of this implicit weighting, Scherrer analysis, when applied to crystallites having a broad size distribution, tends to find a size closer to the high end of the crystallite size range; failing to account for strain in a monodispersed sample, on the other hand, causes Scherrer analysis to yield a size smaller than the actual size of the crystallites. Even analysis of transmission electron microscope (TEM) images may undercount the smallest crystallites, depending on the characteristics of the sample, the criteria used for identifying crystallites, and the imaging technique.

Here, we use extended x-ray absorption fine structure (EXAFS) spectroscopy[5] to estimate the mean crystallite size of a nanocrystalline magnetic material. In the past, this technique has been used to estimate the mean size of nanoparticles, but until now its practical application has generally been limited to nearly monodispersed free particles or to support catalysts of well-defined size and shape. Although EXAFS provides structural information for a region less than a nanometer away from atoms of the element being probed, there will be measurable size effects if the crystallites are less than 10 nm in size, even if the crystal structures are identical. This effect arises because atoms near the boundary of the crystal will be ''missing'' some of their neighbors, and this will thus lower the average coordination numbers in the sample (hereafter called the *termination effect*). Nearly half of the atoms in a 5 nm radius sphere, for example, lie within 1 nm of the boundary; EXAFS would sense a different environment for these atoms than for those in the interior. The termination effect has often been considered a nuisance in EXAFS analysis, because it can easily be confounded by changes in positional (Debye–Waller) disorder or changes in coordination number away from the boundary. In part because of this, several attempts have been made to model it; the most sophisticated have computed atom by atom the effective coordination numbers for specific structures, sizes, and morphologies.[6–9] These analyses are well suited for cases in which the nanocrystals are very small and very regular, and for which the crystal structure is known by other means. The method for estimating crystallite size presented here, in contrast, trades precision for ease of use and range of applicability.

II. SYNTHESIS AND CHARACTERIZATION

A. Synthesis

For this study, we utilized a powder material comprising nanoscale crystallites of fcc nickel in a matrix of body-centered-cubic (bcc) iron within each powder particle. This metal powder consists of polycrystalline spherical particles ranging from approximately 800 nm to 4 μm in diameter,

[a]Electronic mail: scalvin100@aol.com
[b]Present address: Geo-Centers, Fort Washington, MD 20749.

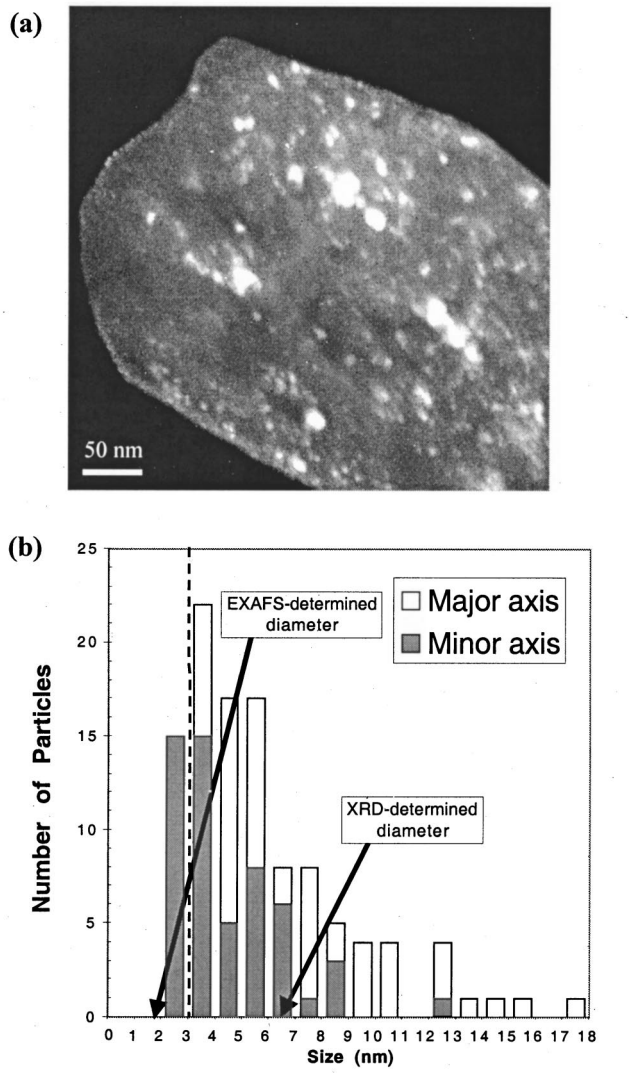

FIG. 1. (a) Dark-field TEM image of a sample showing nickel crystallites (white) in an iron matrix (gray). (b) Histogram of nickel crystallite dimensions from TEM. Crystallites with a major axis smaller than about 3 nm do not have sufficient diffracted intensity to be resolved in this image; this limit is indicated by the dashed line. Note that the EXAFS size indicated is below this limit, and that the EXAFS and XRD determinations establish an interval that includes the majority of the crystallites found by TEM.

produced by an industrial carbonyl process[10] in which $Fe(CO)_5$ and $Ni(CO)_4$ are decomposed in a distillation column at temperatures below 450 °C. The decomposition of nickel carbonyl is faster, so roughly spherical particles of nickel form first. The iron then uses the nickel as nucleation sites, resulting in the incorporation of the nickel particles within an iron matrix.

B. Transmission electron microscopy

Figure 1(a) shows a dark-field TEM image taken of (111) and (200) reflections of nickel crystallites [and also a weak (110) reflection of the bcc iron matrix]. As can be seen, the nickel crystallites are quite polydispersed and, although roughly spherical, often show some distortion in shape, making the atom-by-atom approaches to EXAFS analysis described in Refs. 6–9 difficult to apply. A histogram of crystallite dimensions seen in the TEM is given in Fig. 1(b). Nickel crystallites with major axes smaller than about 3 nm are not expected to have sufficient diffracted intensity to be resolvable here. The number of particles with a major or minor axis of given size rises monotonically with a decrease in size until this limit is reached, suggesting the possibility of numerous crystallites less than 3 nm in diameter.

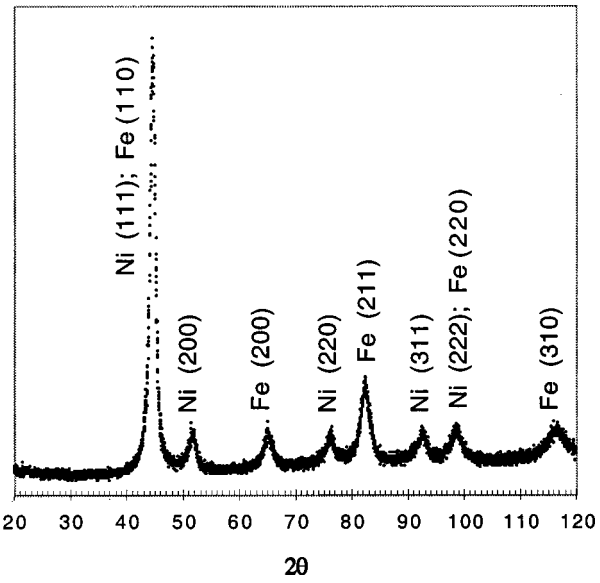

FIG. 2. Diffractogram of a sample with fcc nickel and bcc iron reflections identified.

C. X-ray diffraction

X-ray diffraction (XRD) confirms the presence of fcc and bcc phases (Fig. 2); Scherrer analysis of the peak broadening yields a diameter of 6.4 nm for the nickel particles (the iron peaks are also broadened due to the large number of nickel crystallites that disrupt the lattice). This Scherrer analysis neglects the effects of strain and polydispersion. Strain tends to cause this method to underestimate the actual crystallite size, whereas polydispersion tends to cause overestimation. Examination of Fig. 1(b) suggests that in this case Scherrer analysis yields a size for the nickel crystallites considerably larger than the most probable size, as expected for a polydisperse sample.

D. Magnetic properties

Magnetization measurements of the powder were performed using a DMS model 886 vibrating sample magnetometer (VSM). The powder proved to be a soft ferromagnet with coercive field $H_c \sim 5$ Oe and saturation magnetization M_s of 1140 emu/cm^3. In order to clearly determine the *intrinsic* magnetic properties, sample preparation required special attention. A raw sample of the polydispersed powder consists of not only spherical particles with a range of sizes, but, more importantly for the magnetic properties, nonspherical agglomerations of nearly spherical particles. Scanning electron microscope (SEM) images show many instances of

smaller spheres growing out of larger spheres, suggesting that the agglomerates formed during the carbonyl process. In some cases, the resulting irregularly shaped particles were more than 10 μm across. Since the magnetization process is strongly dependent upon shape, particles smaller than 2 μm were selected for the magnetic measurements, effectively eliminating most of the nonspherical agglomerates.

The magnetization M of a soft (low magnetic anisotropy) ferromagnetic sphere, provided the intrinsic susceptibility is large ($\sim 10/4\pi$ or more in cgs units) can be expressed as[11]

$$M \approx \frac{3}{4\pi} H. \tag{1}$$

This result shows that for *any* spherical, soft (low anisotropy) ferromagnet the magnetization always follows the magnetization curve given by Eq. (1) up to saturation. This saturation field, H_s, is simply related to saturation magnetization M_s by

$$H_s = \frac{4\pi}{3} M_s. \tag{2}$$

To show this magnetization curve a sample of powder was first separated by filtration methods[12] so that the nonspherical agglomerates were largely removed. This filtered powder consisted nearly entirely of spherical polycrystalline particles with average diameters of 0.95 μm and standard deviation of 0.45 μm as determined by SEM. A single sphere of this size at saturation has a magnetic moment on the order of 10^{-10} emu, well below the noise level of the VSM. For this reason, the sample for measurement in the VSM was prepared by ultrasonically dispersing a small amount (~ 85 μg) of this filtered powder in an UV-curing epoxy matrix. The resulting hardened mixture contained a volume fraction on the order of 10^{-5} of fairly well dispersed spheres. When completely dispersed at this low volume fraction, magnetic interaction of the spheres with one another is minimized and magnetization measurements of the ensemble simply reflect the sum of individual sphere magnetizations, thereby providing a net magnetization large enough to be measured above the noise level of the VSM. A magnetization curve of this sample, corrected for the diamagnetic response of the epoxy matrix, is shown in Fig. 3. The dashed line indicates the magnetization curve given by Eq. (1).

From Fig. 3 we see that the individual particles are accurately characterized as soft ferromagnets. This is expected since pure iron carbonyl is known[13–15] to be a soft ferromagnet. The presence of nickel nanograins dispersed throughout the iron matrix should not magnetically harden the material since nickel is also magnetically soft. In addition, as long as the nickel grains are significantly smaller than the magnetic domain wall width, the anisotropy of these grains is effectively averaged out.[1] In such a case, the magnetization of the powder reflects the volumetric average magnetization of the constituent materials.

Analysis by inductively coupled plasma atomic emission spectroscopy[16] showed the actual composition to be $Ni_{30}Fe_{70}$. A homogeneous alloy with this composition would have saturation magnetization of no more than about 500 emu/cm^3,[17] but a phase segregated mixture of bcc iron and fcc nickel should have a value of ~ 1380 emu/cm^3 based on the volume fractions of the constituents.[18] As can be seen in Fig. 3, the measured M_s is within about 17% of this value, suggesting that the fcc phase seen in XRD is primarily nickel, rather than a nickel–iron alloy. This result, combined with the low coercivity of the material, is consistent with nickel nanocrystals embedded in an iron matrix.

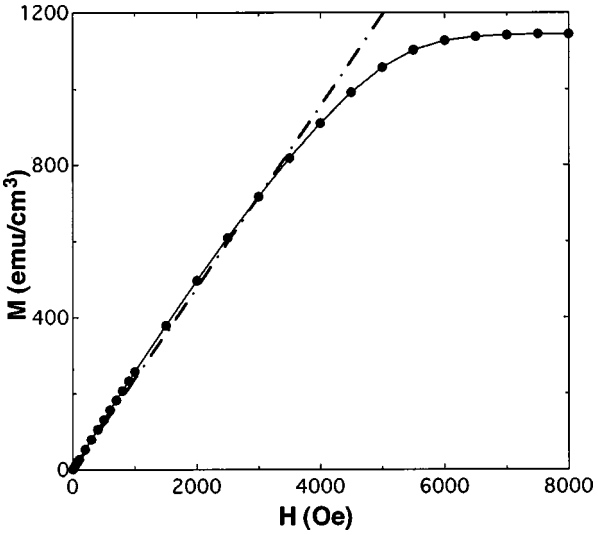

FIG. 3. Magnetization of a diluted (volume fraction $\sim 10^{-5}$) suspension of size-filtered NiFe spheres in epoxy. The curve was corrected for the diamagnetic component of the epoxy. The dashed line shows the idealized magnetization of a soft ferromagnetic sphere that is dominated by demagnetization.

E. X-ray absorption spectra

To prepare a sample for EXAFS data collection, the powder was ground in a mortar by a pestle, and then applied as thin layers to Kapton tape. The number of layers of tape was chosen so that the total absorption was approximately 0.7 at the nickel K edge and 1.9 at the iron K edge. Nickel and iron K-edge x-ray absorption spectra of the sample were collected at beam line X11A at the National Synchrotron Light Source at Brookhaven National Laboratories; uniformity was confirmed at the beam line by measuring the transmission as a function of the beam position. Simultaneously, spectra of iron and nickel foils were collected as reference samples. Two scans were averaged to evaluate and reduce random noise; the resulting spectra are shown in Fig. 4.

III. ANALYSIS AND DISCUSSION

A. Data reduction

Background subtraction following the prescription of Newville *et al.*[19] was performed on all spectra, using a spline to minimize non-EXAFS features below 0.09 nm in the Fourier transform. After background subtraction and normalization by the edge jump, the data were transformed to a function of photoelectron wave number k. Since the EXAFS amplitude generally falls off with an increase in k, the data were multiplied by k^2 (Fig. 5) prior to taking the Fourier transform (Fig. 6).

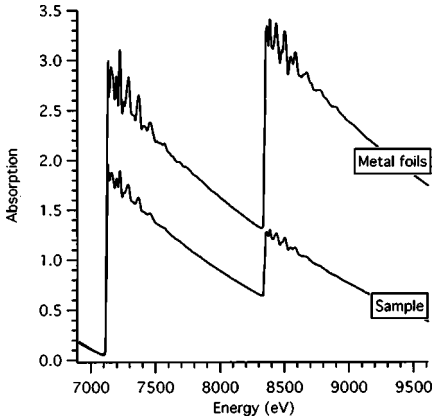

FIG. 4. X-ray absorption spectra of iron (7112 eV) and nickel (8333 eV) *K* edges of reference foils and the sample. The spectra were translated vertically for display purposes.

The Fourier transform, although related to the radial distribution function about the absorbing element, is modified by several factors such as the potential of the absorbing and scattering atoms, the core–hole lifetime, and effects due to multiple scattering.[5] The result is that, although major peaks can be identified as due to particular scattering shells, they are typically shifted from 0.01 to 0.05 nm toward lower *r*. In addition, the Fourier transform itself can introduce spurious sidebands due to the discontinuity between the first and last points in the selected data. This latter effect is conventionally reduced (but not eliminated) by applying a window function to the weighted *k*-space spectra prior to transforming, so that the spectra fall smoothly to zero at the endpoints. In addition, the implementation of fast Fourier transforms on digital computers often imposes a practical limitation in that the number of selected data points is a power of two; windowing allows the selected data to be ''padded'' with zeros without significantly affecting the transform. In this study, a Hanning window with sills 10 nm^{-1} wide was used. For the purposes of the technique described here, it is desirable to further minimize sidebands by choosing starting and ending points for the selected data such that their values are already close to zero before windowing; a range of 32.5–104.0 nm^{-1} was used for the nickel data.[20]

Comparison to the reference spectra confirmed that in this material the nickel is in a fcc structure and the iron is in a bcc structure, in agreement with the TEM imaging, diffraction, and magnetic analyses.

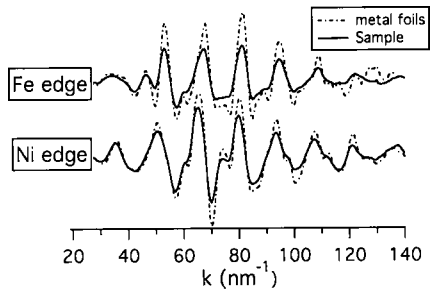

FIG. 5. EXAFS spectra (weighted by k^2) of the sample and reference foil for iron and nickel *K* edges.

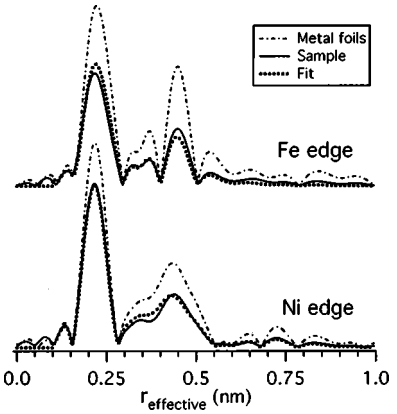

FIG. 6. Magnitude of Fourier transforms of the sample and reference foil data for iron (top) and nickel (bottom) *K* edges. ''Fit'' applies the termination model to foil transform to approximate the sample transform. Note the substantial mismatches in the Fe fit at the major peaks near 0.2 and 0.45 nm; these are probably due to the nonspherical morphology of the iron matrices. The fit to the Ni spectrum is considerably better.

B. Size of nickel crystallites

Inspection of Fig. 6 reveals that, although the peaks of the Fourier transform for the sample and the reference are in very similar positions, the amplitude is substantially smaller for the sample. Furthermore, the reduction is fractionally greater at larger r_{eff}. This can be explained on the basis of the termination effect: the average coordination number is reduced due to atoms near the boundary; the effect is naturally greater for shells of scattering atoms that lie at greater distances from the absorbing atom.

To model the effect, we considered the case of a homogeneous spherical crystallite of radius *R* (Fig. 7). For an atom a distance ρ from the center of the crystallite, a scattering path of length *r* has its amplitude reduced, relative to that of a bulk standard, by a factor equal to the fraction of the surface area of the scattering sphere (radius *r*) that is contained within the crystallite (radius *R*):

$$\frac{R^2-(\rho-r)^2}{4\rho r}. \tag{3}$$

Integrating through the crystallite sphere and dividing by its volume yields the reduction in average coordination number relative to the bulk:

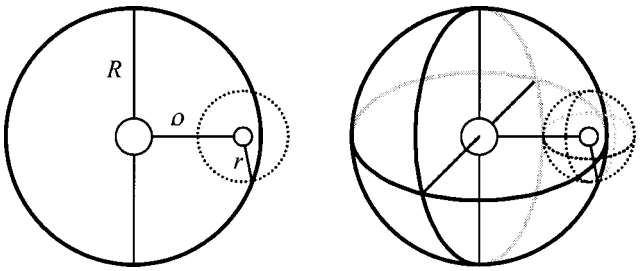

FIG. 7. Spherical homogeneous model. *R* is the radius of the crystallite, ρ is the distance from the center of the crystallite to the absorbing atom, and *r* is the distance from the absorbing atom to the scattering. By integrating the portion of the volume of the small sphere which is within the large sphere over all values of ρ less than *R* and normalizing by the volume of the large sphere, the magnitude of the termination effect can be approximated.

$$N_{\text{nano}}=\left[1-\frac{3}{4}\left(\frac{r}{R}\right)+\frac{1}{16}\left(\frac{r}{R}\right)^3\right]N_{\text{bulk}}. \quad (4)$$

Since the amplitude of the peaks in the Fourier transform at a given distance is proportional to the coordination number, this gives the reduction in peak amplitude. This formula was used to determine R for the nickel edge by fitting the sample Fourier transform to the reference Fourier transform modified by this formula.[21] For the nickel edge, the result gave an excellent fit (see Fig. 6) when R was 0.88 nm, implying a diameter of about 1.8 nm.[22] Although this value is considerably smaller than that indicated by Scherrer analysis, this technique is more sensitive to small crystallites, whereas Scherrer analysis is more sensitive to large crystallites. As mentioned above, the TEM shows increasing numbers of crystallites of smaller size until the intensity/resolution limit is reached (for these dark-field imaging conditions) at around 3 nm, and is thus consistent with the EXAFS result.

It should be emphasized that, like Scherrer analysis, this technique provides only a rough estimate of the crystallite size. It should not be regarded as equal in accuracy to high-resolution TEM or EXAFS determinations based on atom-by-atom models. It can, however, be applied easily to a wide range of samples and, unlike other EXAFS determinations, it requires neither a theoretical standard nor a multivariable fit. A bulk standard is necessary, but the atomic structure of this standard does not need to be known.[23]

C. Limitations of the model

Because this is an approximate technique, it is important to consider its limitations.

(1) To the extent that the crystallites are not spherical, Eq. (4) will be inaccurate. This is most pronounced for shapes with high boundary to volume ratios, such as needles. If a particular nonspherical morphology is suspected, it is straightforward to develop an equation analogous to Eq. (4).
(2) If the size distribution of the crystallites is broad, this method will yield a result that is heavily weighted toward the low end of the distribution. For example, applying this technique to a bimodal distribution in which 50% of the atoms were in particles 2 nm in diameter and 50% were in particles 15 nm in diameter would yield a ''mean'' diameter of approximately 3.5 nm.
(3) r_{eff} is not the actual distance from absorber to scatterer. In this work, the peaks for the bulk spectra were examined and compared to the known distances in the materials; an average offset of -0.03 nm was found. To correct for this 0.03 nm was added to each r_{eff} prior to fitting in order to approximate the shift. The effect of this correction on the value of R determined by the fits was less than 0.03 nm.
(4) Multiple-scattering contributions are not properly accounted for in this scheme, since it is assumed that r_{eff} is ''similar to'' the distance from the absorbing atom to the scattering atom. In the case of a multiple-scattering path that scatters off two nearest neighbors, for example, the contribution occurs at a r_{eff} as much as twice that of the direct scattering path off a nearest neighbor.
(5) Sidebands and peak broadening due to specifics of the Fourier transform may distort the dependence of the relative amplitude on r_{eff}. For this reason, it is preferable to choose a range of data to Fourier transform that already goes nearly to zero at the endpoints, rather than relying solely on windows. For the sample we examined, the effect was small but not negligible; it changed the determination of R by less than 0.1 nm in all cases.

These effects, while important, are no more severe than the limitations imposed on Scherrer analysis of x-ray diffractograms by phenomena such as instrumental broadening and strain. In addition, the most significant effects act together to reduce the crystallite size determined by this method, making it a fairly reliable lower limit for the mean crystallite size. Confidence in sizes obtained in this way is increased by also performing Scherrer analysis, since for polydispersed samples the EXAFS and Scherrer sizes will generally bracket the sizes of the majority of crystallites.

D. Application to iron matrix

As an example of a sample where the limitations described above are more significant, we investigated the iron spectrum of the same sample. In contrast to the nickel phase, a nanoscale spherical model is manifestly unsuitable for the morphology of the iron matrix, since the matrix consists of micron-scale crystals that contain multiple nanoscale defects of roughly spherical shape (the nickel crystallites). Nevertheless, it is instructive to consider the effect of applying the spherical model to this phase, since the morphology of nanoscale materials is not always known. Using a k range of 30.0–105.5 nm^{-1},[24] the fit yielded a value of 0.57 nm for R.[25] As can be seen in Fig. 6, the quality of the fit is considerably worse than that for the nickel spectrum, as expected.

Scherrer analysis of the iron phase yields a mean diameter of 5.4 nm for the iron. Scherrer broadening suffers from the same morphological effects as EXAFS analysis, but the weighting is quite different. As discussed above, the mean diameter determined by XRD is weighted heavily toward the larger distances in the distribution. Thus, for nonspherical particles modeled as spherical ones, XRD will yield a distance close to the maximum diameter of the crystallites. EXAFS, on the other hand, is weighted more toward the smaller distances in the distribution. For nonspherical particles, the difference between the XRD and EXAFS determined ''diameters'' will therefore be exaggerated. In the case of the iron phase, Scherrer analysis indicates the iron crystallite diameter is 84% that of nickel, whereas EXAFS indicates that the ratio is 65%.

The consistency of the size scales for the nickel crystallites and the iron matrix can be confirmed by making an order-of-magnitude estimate of the distance between nickel crystallites, e.g., if they were monodispersed and evenly distributed. For 1.8 nm diameter nickel crystallites distributed on a close-packed lattice, the stoichiometry of the sample would dictate that the centers of the nearest-neighbor nickel

crystallites would be 2.4 nm apart. This would place the *surfaces* of the crystallites 0.6 nm apart at their nearest point, in agreement with the distance scale assigned to the iron matrix by EXAFS.

IV. CONCLUSIONS

In summary, it is possible to estimate the size of nanocrystals of known composition by comparing the amplitude of the EXAFS with that of a reference material. The model works best with phases from 1 to 10 nm nanometers in diameter; for clusters of atoms less than 1 nm in diameter the spherical approximation and the need for a similar bulk crystal limit its usefulness, while for particles more than 10 nm in diameter the termination effect becomes quite small. While the technique is not as accurate as high-resolution TEM imaging for appropriate samples, it is possible to utilize it in situations where TEM is prohibitively difficult, such as *in situ* time-resolved studies, when (as here) nanocrystallites of similar contrast are buried within a thick matrix, or when a statistically large sample size is desired. In addition, the technique offers advantages over Scherrer analysis of XRD: it is element specific (allowing, for example, the discrimination of fcc cobalt crystallites in a fcc nickel matrix) and it is weighted more toward the smaller end of the size distribution than XRD, thereby enhancing its usefulness as a complement to TEM. It may also be used to improve EXAFS analyses that utilize curve fitting to an empirical standard by providing an easily implemented first-order correction to account for the termination effect.

ACKNOWLEDGMENTS

The authors wish to thank Lynn Kurihara, Peter Lubitz, Bruce Ravel, Jess Riedel, George Spanos, and Matt Willard of the Naval Research Laboratory, Kumi Pandya of the Naval Research Laboratory Synchrotron Radiation Consortium, and Lou Koehler of Novamet for their assistance with this project. Financial support was provided by DARPA/DSO and ONR.

[1] M. E. McHenry, M. A. Willard, and D. E. Laughlin, Prog. Mater. Sci. **44**, 291 (1999).
[2] R. Pecora, J. Nanopart. Res. **2**, 123 (2000).
[3] S. Brunauer, P. H. Emmett, and E. Teller, J. Am. Chem. Soc. **60**, 309 (1938).
[4] R. Zsigmondy, *Kolloidchemie*, 3rd ed. (Spamer, Leipzig, 1920).
[5] J. J. Rehr and R. C. Albers, Rev. Mod. Phys. **72**, 621 (2000).
[6] R. B. Greegor and F. W. Lytle, J. Catal. **63**, 476 (1980).
[7] A. I. Frenkel, C. W. Hills, and R. G. Nuzzo, J. Phys. Chem. B **105**, 12689 (2001).
[8] I. Arcon, A. Tuel, A. Kodre, G. Martin, and A. Barbier, J. Synchrotron Radiat. **8**, 575 (2001).
[9] C. J. Riedel, S. Calvin, E. E. Carpenter, R. M. Stroud, C. M. Larkin, R. Y. Williams, and V. G. Harris (unpublished).
[10] F. L. Ebenhoch, in *Physical Chemistry of Powder Metals Production and Processing*, edited by W. M. Small (The Minerals, Metals, and Materials Society, Warrendale, PA, 1989), p. 271.
[11] M. Miller, P. Sheehan, R. Edelstein, C. Tamanaha, L. Zhong, S. Bounnak, L. Whitman, and R. Colton, J. Magn. Magn. Mater. **225**, 138 (2001).
[12] The dry powder was shaken vigorously over a polycarbonate filter (5 μm pore size) for several hours. UV curable epoxy was added to a small amount of the size-selected powder and sonicated in a water bath for 20 min. The epoxy was then exposed to 365 nm UV light and allowed to cure for 1 h.
[13] J. Ding, Y. Shi, L. F. Chen, C. R. Deng, S. H. Fuh, and Y. Li, J. Magn. Magn. Mater. **247**, 249 (2002).
[14] R. M. Bozorth, *Ferromagnetism* (Van Nostrand, New York, 1951), p. 870.
[15] S. Chikazumi, *Physics of Magnetism* (Krieger, Malabar, FL, 1978), p. 498.
[16] R. H. Wendt and V. A. Fassel, Anal. Chem. **37**, 920 (1965).
[17] The saturation magnetization of Ni–Fe alloys as a function of the Ni content has a sharp minimum of ~300 emu/cm^3 at 30% Ni; see Ref. 14, p. 113.
[18] The saturation values of elemental Ni and Fe are taken to be 485 and 1710 emu/cm^3, respectively; see Ref. 15, pp. 19 and 494.
[19] M. Newville, P. Livins, Y. Yacoby, J. J. Rehr, and E. A. Stern, Phys. Rev. B **47**, 14126 (1993).
[20] Conventionally, k ranges are written as if the data were bounded by the middle of each Hanning windowsill. Here, the range is written to the edges of the sills to emphasize that the function is close to zero at these points. In conventional notation, this range would be written as 37.5–99.0 nm^{-1}.
[21] The fit was for the Fourier transform above 0.1 nm, since background subtraction modifies the Fourier transform below that point.
[22] It is certainly possible for nanoscale crystallites to differ from their bulk counterparts in ways other than simple termination. In such a case, it is likely that the one-parameter fit used here would simply fail to reproduce the data. Since the effects of common variations such as those in the first, second, and third EXAFS cumulants are weighted by powers of k, we considered it prudent to guard against this possibility by repeating the procedure at different k weights; that is, we multiplied the data by k and k^3 prior to taking Fourier transforms, in addition to the k^2 weighting described in the text. The results were largely unchanged, yielding values of R of 0.92 and 0.84 nm, respectively. The quality of the fits was similar in all cases.
[23] For soft magnetic materials that have technological applications, it is unlikely that the structure of the bulk reference material is unknown. This technique is not limited to this category of materials, however. Environmental samples, for example, often contain nanocrystallites of minerals that are routinely identified by XRD and yet have unknown atomic structures.
[24] 35.0–100.5 nm^{-1} in conventional notation (see Ref. 20).
[25] k-weight 1 and 3 fits produced values of 0.60 and 0.55 nm, respectively.